



Comprehensive Analysis of Serum Metabolites Profiles in Acute Radiation Enteritis Rats by Untargeted Metabolomics

He Nie,^{1,*} Jiadong Pan,^{1,*} Fangmei An,¹ Chuwei Zheng,¹ Qinglin Zhang¹ and Qiang Zhan¹

¹Department of Gastroenterology, Wuxi People's Hospital Affiliated to Nanjing Medical University, Wuxi, China

Acute radiation enteritis is a common complication occurring in patients with pelvic and abdominal tumors who receive radiotherapy. Acute radiation enteritis seriously reduces the life quality, even threatens the lives of patients. Untargeted metabolomics is an emerging strategy to explore the novel biomarkers and uncover potential pathogenesis of acute radiation enteritis. Acute radiation enteritis rat model was established by single abdominal irradiation with a gamma-ray dose of 10 Gy. Serum from 15 acute radiation enteritis rats and 10 controls was extracted for metabolomics analysis by UHPLC-Q-TOF/MS. Clinical manifestations and morphological alterations of intestine confirmed the successful establishment of acute radiation enteritis. According to the metabolomics data, 6,044 positive peaks and 4,241 negative peaks were extracted from each specimen. OPLS-DA analysis and the heat map for cluster analysis showed satisfactory discriminatory power between acute radiation enteritis rats and controls. Subsequent analysis extracted 66 significantly differentially expressed metabolites, which might be potential biomarkers for acute radiation enteritis diagnosis. Moreover, Kyoto Encyclopedia of Genes and Genomes enrichment analyses uncovered the potential mechanisms through which differentially expressed metabolites participated in acute radiation enteritis pathogenesis. To sum up, we summarized several differentially expressed serum metabolites as potential biomarkers for diagnosis of acute radiation enteritis and provide latent clues for elucidating acute radiation enteritis pathology.

Keywords: acute radiation enteritis; animal model; biomarkers; metabolomics; pathogenesis
Tohoku J. Exp. Med., 2021 November, 255 (3), 257-265.

Introduction

Radiotherapy is commonly used in comprehensive treatment for common malignancies (Abshire and Lang 2018). For radiotherapy of gastrointestinal cancer, ionizing radiation is often administrated to patient's abdomen or pelvis (Stacey and Green 2014). However, abdominal and pelvic radiation can cause several typical and complex damages in the bowel tissues, which are always known as acute radiation enteritis (ARE). Without treatments, more severer symptoms will develop, such as intestinal fibrosis, intestinal stenosis or perforation, anorectal fistula and intestinal adhesion (Ashburn and Kalady 2016). In patients who received abdominal or pelvic radiotherapy, about 90% developed

changes in their bowel habit, and life quality of more than 50% patients was impacted profoundly by ARE (Khalid et al. 2006). The diagnosis of ARE is suspected in patients with nausea, vomiting, abdominal pain, diarrhea, or lower gastrointestinal bleeding after completion of radiotherapy, and established by endoscopy and histology (Hauer-Jensen et al. 2007). However, because endoscopy and histopathologic examinations can cause further injury and discomfort, non-invasive methods are necessary to diagnose ARE.

Because ARE often disrupts metabolism and absorption function of the bowel system, serum levels of certain metabolites change in ARE patients compared to healthy people. Therefore, identification of those differential metabolites will be highly promising to establish diagnostic

Received May 24, 2021; revised and accepted August 24, 2021. Published online December 1, 2021; doi: 10.1620/tjem.255.257.

*These two authors contributed equally to this work.

Correspondence: Qiang Zhan, M.D., Department of Gastroenterology, Wuxi People's Hospital Affiliated to Nanjing Medical University, No. 299 Qing Yang Road, Wuxi 214023, China.

e-mail: ryzhanqiang@163.com

Qinglin Zhang, M.D., Department of Gastroenterology, Wuxi People's Hospital Affiliated to Nanjing Medical University, No. 299 Qing Yang Road, Wuxi 214023, China.

e-mail: zhang517068@126.com

©2021 Tohoku University Medical Press. This is an open-access article distributed under the terms of the Creative Commons Attribution-NonCommercial-NoDerivatives 4.0 International License (CC-BY-NC-ND 4.0). Anyone may download, reuse, copy, reprint, or distribute the article without modifications or adaptations for non-profit purposes if they cite the original authors and source properly.
<https://creativecommons.org/licenses/by-nc-nd/4.0/>

biomarkers for ARE. Among various methods applied to assess the metabolites (including mass spectrometry, untargeted metabolomics, targeted metabolomics and imaging metabolomics) (Johnson et al. 2016), metabolomics approach is the most powerful due to its rapid, high throughput and sensitive characteristics (Pannkuk et al. 2017). So far, several studies have identified some metabolomic biomarkers for radiation injury through animal models (Zhang et al. 2014; Jones et al. 2017; Zhao et al. 2017). For example, Laiakis et al. (2012) revealed that radiation injury led to significant change in metabolites of tricarboxylic acid and fatty acids cycle in the urine. Compared with biomarkers in the urine, bioindicators in the serum are more reliable. Several studies demonstrated that serum profiling of metabolites relating to the pyrimidine and tryptophan pathways could be used as candidate indicators of radiation exposure (Ni et al. 2008; Broin et al. 2015). However, all those studies were based on total-body irradiated animal models, and the metabolomics changes in partial radiation-induced ARE models have not been investigated yet.

In the current research, we established a physiologically relevant ARE rat model and analyzed the differentially expressed serum metabolites between ARE and normal rats. We identified 66 significantly differentially expressed metabolites. As a result, we summarized several differentially expressed serum metabolites as potential biomarkers for diagnosis of ARE. In addition, we provided novel insights into the pathology of ARE.

Materials and Methods

Animal model

Adult male Sprague-Dawley (SD) rats (7-8 weeks) weighing 220-250 g were purchased from Shanghai SLAC Laboratory Animal Co. Ltd (Shanghai, China). All rats were housed in the room maintained at constant temperature and humidity with a 12/12 h light/dark cycle according to the guidelines established by Nanjing Medical University. All experimental procedures were approved by the Supervisory Committee of Nanjing Medical University Animal Council. A total of 25 SD rats were randomly divided into two groups including 10 rats in control group and 15 in ARE group. ARE rat model was established through single abdominal irradiation with a gamma-ray dose of 10 Gy at a rate of 500 cGy/min, while rats in normal group received mock radiation. The fecal condition of each rat was recorded. After the radiation, 4 mL of whole blood was drawn from each rat, and then the rat was euthanized by excessive sodium pentobarbital injection. Hematoxylin and eosin (H&E) staining was applied to assess the alterations in intestinal structure at four days after radiation.

Serum samples preparation

At 4 days after the radiation, 4 mL of whole blood was drawn from each rat. The whole blood was extracted into anticoagulant-treated tubes. Cells in the whole blood were

removed by centrifugation at 4°C (15 min, 2,000 × g). The supernatant was transferred to sterilized polypropylene tubes. Afterwards, 100 µL of supernatant was taken and mixed with 400 µL of ice-cold methanol/acetonitrile (1:1, v/v). The protein in the mixture precipitated out after incubation at -20°C for 1 hour. Protein precipitation was removed by centrifugation at 4°C (20 min, 14,000 × g). After the centrifugation, the supernatant was lyophilized and stored at -80°C. Before UHPLC-Q-TOF/MS, the sample was dissolved in 150 µL of ice-cold mixture of methanol and acetonitrile (1:1, v/v) with 10 µL of internal standard (0.3 mg/mL 2-chloro-1-phenylalanine in methanol). Subsequently, according to Chen et al. (2013), the mixture was ultrasonicated at room temperature for 5 min, followed by incubation at -20°C for 10 min. After that mixture was centrifuged at 4°C (12,000 × g, 10 min). A total of 100 µL of supernatant from each tube was collected, filtered through 0.22 µm microfilters, and transferred to LC vials.

UHPLC-Q-TOF/MS analysis

Metabolic profiling of serum specimens was analyzed with an Agilent 1290 infinity LC system coupled with an AB SCIEX Triple time-of-flight 5600 system. Columns (Waters, ACQUITY UPLC BEH Amide 1.7 µm, 2.1 mm × 100 mm and Waters, ACQUITY UPLC HSS T3 1.8 µm, 2.1 × 100 mm) were employed. Serum samples were separated by chromatography with the column temperature at 25°C. The mobile phase consisted of 25 mM ammonium acetate and 25 mM ammonia in water (A) and acetonitrile (B). The elution gradient initially was initiated with 95% B for 1 min, linearly decreased to 65% B at 14 min, maintained for 2 min, and then returned to 95% B for 2 min of equilibrium. The delivery flow rate was 300 µL/min, and 2 µL of aliquot of each sample was injected into the column. Time of flight (TOF)/MS was performed on both positive ion mode and negative ion mode.

Electrospray ionization (ESI) source conditions were set as follows: ion source gas 1, 60 psi; ion source gas 2, 60 psi; curtain gas, 30 psi; source temperature, 600°C; ion-spray voltage floating, ± 5,000 V; TOF MS scan m/z range, 60-1,000 Da; product ion scan m/z range, 25-1,000 Da; TOF/MS scan accumulation time, 0.20 s/spectra; product ion scan accumulation time, 0.05 s/spectra. MS/MS spectra were acquired with information dependent acquisition (IDA) in high sensitivity mode. The parameters were set as follows: declustering potential, ± 60 V; collision energy, 35 ± 15 eV; exclude isotopes within 4 Da; and candidate ions to monitor per cycle, 6.

Metabolomics data analysis

The raw UHPLC-Q-TOF/MS data were converted to mzXML files and then processed online using XCMS software. The structures of metabolites were established by searching the support database with accurate mass match ($\Delta m/z < 25$ ppm) and MS/MS spectra comparison. The XCMS data were processed by Pareto-scaling with

SIMCA-P 14.1 software. Principle component analysis (PCA) was conducted and a heat map of hierarchical clustering analysis was generated for the unsupervised multivariate statistical analysis. Orthogonal partial-least squares discrimination analysis (OPLS-DA) was conducted as a supervised method to identify the important variables with discriminative power, and OPLS-DA model was validated by a permutation test with 200 iterations. The variable importance in the projection (VIP) value of each variable in the OPLS-DA model was calculated to display its contribution to the classification. Metabolites with the VIP value > 1 were further applied to Student's t-test at univariate level to measure the significance of each metabolite. $P < 0.05$ was considered as statistical significance.

To evaluate the differentially expressed metabolites, Hierarchical Clustering assay was applied to analyze the expression mode of metabolites. We further conducted the metabolomics pathway analysis with the differentially expressed metabolites by Kyoto Encyclopedia of Genes and Genomes (KEGG) analysis.

Results

Rat model for radiation-induced acute radiation enteritis (ARE)

Two days after radiation, ARE rats exhibited obvious diarrhea, but the control rats still defecated normally. Compared to control rats, abdominal irradiation caused

obvious edema of intestinal wall and the intestinal contents became thinner (Fig. 1A, B). Further H&E staining indicated a dramatic destruction in the intestinal villi of irradiated animals, whereas the intestinal villi of control rats kept smooth and intact (Fig. 1C, D), which was consistent with Li's findings (Li et al. 2017b). All these results confirmed the occurrence of ARE.

Quality control of untargeted metabolomics analysis

We applied Pareto scaling and 7-fold cross-validation to establish the PCA model using the molecular features of all the groups from the study, including quality control (QC) samples. The distribution of metabolic profiles for the test samples and QC samples in PCA is exhibited in Fig. 2. All the QC injections were clustered tightly in PCA space. The consistency of the repeated QC injections and reliable data quality across all the specimens uncovered the potency of the metabolic profiling strategy during the experiment. In the end, 6,044 positive peaks and 4,241 negative peaks were extracted using XCMS software.

Untargeted metabolomics analysis of serum obtained from control and ARE rats

Before analyzing the differentially expressed metabolites, we first validated the algorithm model used in this study by OPLS-DA. As shown in the score plots of OPLS-DA model, clear separation between ARE and nor-

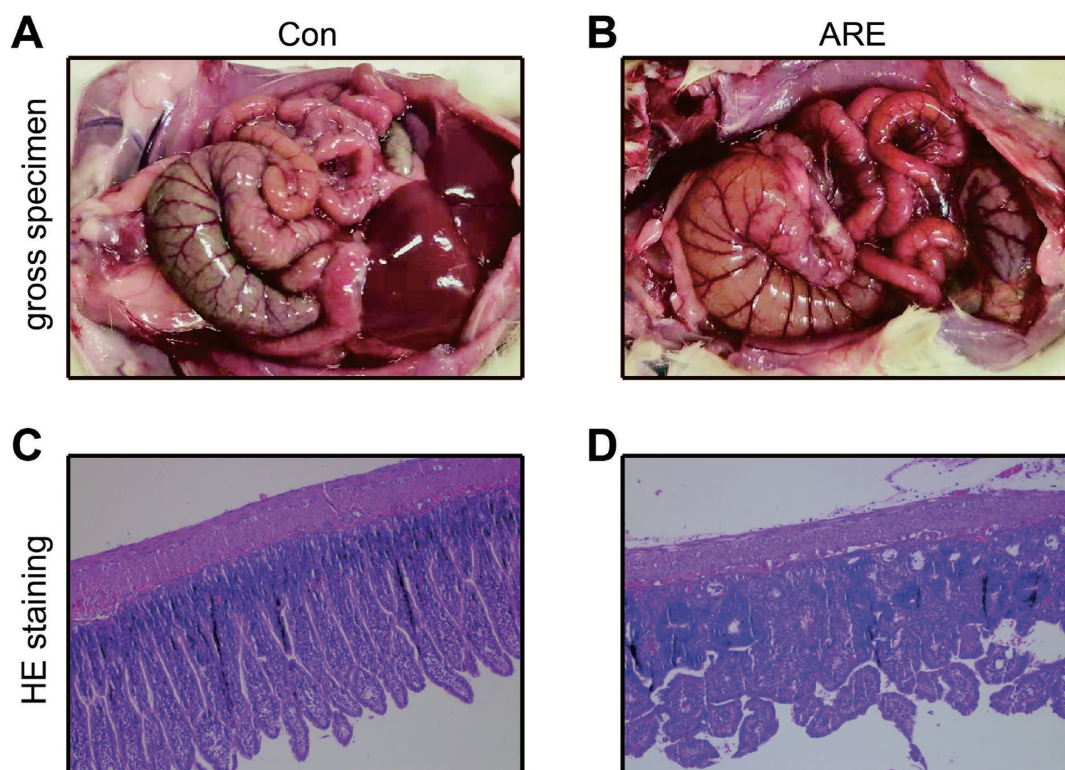


Fig. 1. Difference in bowel morphology between normal (CON) and acute radiation enteritis (ARE) rats. The morphological changes of intestine after four days of radiation. (A, B) Macroscopic images of intestine of representative normal and ARE rats. (C, D) Intestine structure of a representative normal and ARE rats, (H&E staining, $\times 100$).

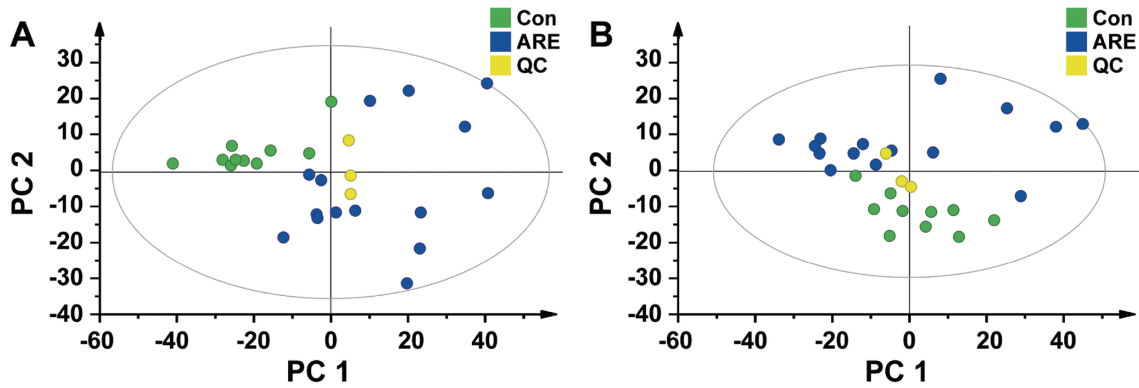


Fig. 2. Principle component analysis (PCA) score plots based on the UHPLC-Q-TOF/MS data of serum samples. The distribution of metabolic profiles for the test samples and quality control (QC) samples in PCA. (A) Positive ion mode; (B) Negative ion mode. Con, normal rats; ARE, acute radiation enteritis rats; Q2, predictive ability; R2, goodness of fit.

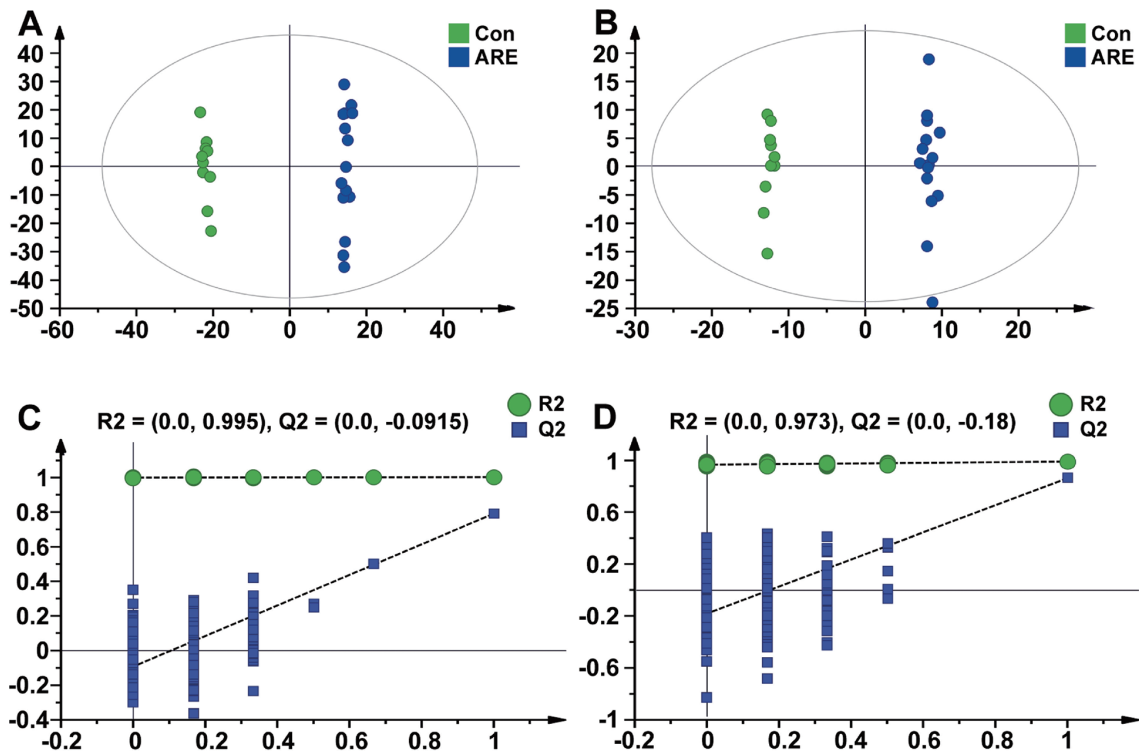


Fig. 3. Multivariate statistical analysis of metabolomics between normal (CON) and acute radiation enteritis (ARE) rats. Orthogonal partial-least squares discrimination analysis (OPLS-DA) score plot derived from UHPLC-Q-TOF/MS-based metabolomics analysis between normal (green circles) and ARE rats (blue circles). (A) Positive ion mode; (B) Negative ion mode. Statistical validation of the OPLS-DA model by permutation testing. (C) Positive ion mode; (D) Negative ion mode.

mal control groups was observed (Fig. 3A, B). Specifically, the explanation rates for Y variable (R2Y) and prediction ability (Q2) were 0.998 and 0.788 in positive ion mode, and 0.997 and 0.866 in negative ion mode, respectively, which confirmed the stability and reliability of the OPLS-DA model. Moreover, the cross-validation through permutations tests (200 times) validated no overfitting of the models (generated intercepts of $R2 = 0.995$, $Q2 = -0.0915$ and $R2 = 0.973$, $Q2 = -0.18$ for positive and negative ion mode, respectively) (Fig. 3C, D). The heat map of hierarchical

clustering analysis was another useful tool to evaluate the relationship among samples as OPLS-DA model, and reveal the expression differences of metabolites intuitively. In Fig. 4, we can see the similarity between the metabolite abundance profiles, exhibiting a satisfactory discriminatory value between the two groups.

Table 1. Metabolites changed in acute radiation enteritis (ARE) model (positive ion mode).

| Name | Description | VIP | Fold change | P-value |
|------------|--|---------|-------------|-------------|
| M138T542 | Anthranilic acid (Vitamin L1) | 2.35104 | 0.105056798 | 8.46548E-15 |
| M426T426 | Cholic acid | 1.539 | 0.223951201 | 0.000109244 |
| M190T201 | 1H-Indole-3-propanoic acid | 1.63636 | 0.260969767 | 3.69516E-07 |
| M468T367 | 1-Myristoyl-sn-glycero-3-phosphocholine | 1.09014 | 0.344706634 | 1.30692E-11 |
| M360T754 | Cellobiose | 2.84827 | 0.365165177 | 1.4588E-05 |
| M757T266 | PC (16:0/16:0) | 1.31477 | 0.452339803 | 5.80328E-06 |
| M787T98 | 1,2-dioleoyl-sn-glycero-3-phosphatidylcholine | 2.1203 | 0.50182228 | 7.71342E-06 |
| M522T340 | 1-Oleoyl-sn-glycero-3-phosphocholine | 1.59205 | 0.518717984 | 2.62806E-09 |
| M123T104 | Nicotinamide | 1.33369 | 0.522335307 | 3.59305E-05 |
| M568T334 | 1-Stearoyl-sn-glycerol 3-phosphocholine | 1.06744 | 0.527817393 | 8.50122E-08 |
| M568T347_2 | 1-Stearoyl-2-hydroxy-sn-glycero-3-phosphocholine | 2.90213 | 0.580982355 | 2.46018E-06 |
| M759T140 | Thioetheramide-PC | 4.0512 | 0.634027766 | 0.041542231 |
| M116T591 | D-Proline | 1.58999 | 0.746984412 | 0.000318848 |
| M496T358_6 | 1-Palmitoyl-sn-glycero-3-phosphocholine | 7.56858 | 0.753737104 | 0.001989698 |
| M134T56 | Oxindole | 1.1627 | 0.755107192 | 0.024023081 |
| M127T184 | Thymine | 2.15351 | 0.75949722 | 0.042436024 |
| M198T586 | D-Mannose | 2.1822 | 0.788858491 | 0.029244988 |
| M162T702 | L-Carnitine | 2.33122 | 0.803923678 | 0.024431148 |
| M204T581_1 | Acetylcarnitine | 1.30131 | 1.36286635 | 2.46186E-05 |
| M213T806 | Triethanolamine | 1.36728 | 1.448326428 | 0.021307703 |
| M263T495_2 | L-Norleucine | 1.43561 | 1.454400984 | 0.009826322 |
| M380T531 | D-erythro-Sphingosine-1-phosphate | 1.8936 | 1.549194113 | 0.000185891 |
| M331T481 | DL-Phenylalanine | 1.58168 | 1.599719782 | 0.010297971 |
| M133T718 | L-Asparagine | 2.54643 | 1.711577394 | 1.59898E-05 |
| M112T456 | Cytosine | 2.25701 | 1.776507878 | 5.20017E-05 |
| M276T732 | L-Pyroglutamic acid | 1.79598 | 1.791179823 | 0.002031896 |
| M245T305 | Uridine | 1.57054 | 1.84170737 | 0.04745144 |
| M216T756 | sn-Glycerol 3-phosphoethanolamine | 1.60052 | 1.998519718 | 0.008724778 |
| M104T511 | Choline | 1.5913 | 2.074146034 | 0.009726898 |
| M811T137 | 1-Stearoyl-2-oleoyl-sn-glycerol 3-phosphocholine | 1.59529 | 2.363577649 | 0.014745039 |
| M132T703 | Creatine | 1.90859 | 2.492152245 | 0.003800136 |

VIP, the variable importance in the projection.

dictive value in diagnosis of type 1 diabetes mellitus and schizophrenia (Oxenkrug et al. 2015, 2016), but literature reporting its role in radiation injury is not available. Hippuric acid is a major human metabolite, which has been reported as a potential indicator for diabetic kidney disease and multiple sclerosis (Li et al. 2017a; Atya et al. 2018). Hippuric acid is also shown to be related to hepatic radiation injury (Kurland et al. 2015). Gut microbiome abnormalities may cause metabolic disorders (Fan and Pedersen 2021). The abnormal metabolites above may be related to the changes of gut microbiome (Nicholls et al. 2003).

To get a better view of the overall profile of metabolites in ARE, we conducted the metabolomics pathway analysis with the differentially expressed metabolites by KEGG enrichment analysis. We found that most metabolites were enriched into 14 pathways, including central carbon metabolism in cancer, mineral absorption, protein

digestion and absorption and so on. Among them, ABC transporters had the greatest number of overlapped compounds. ABC transporters have been identified in many metabolomics studies on different diseases (Alakwaa et al. 2018; Liu et al. 2019). According to the previous literature, ABCA1, a key member of ABC transporters, has point mutation R219K that participates in the mechanisms of radiation-induced dermatitis (Isomura et al. 2008). Their article revealed that ABC transporters might participate in the mechanisms of radiation-induced injury, which is accordant with our findings. Besides, other pathways also exhibited preliminary association with the development of ARE.

This study has several limitations. First, the sample size was small with just 25 SD rats. If more samples are available, more satisfactory results may be obtained. Second, we just analyzed the serum metabolites profiles by untargeted metabolomics, and if comparative analysis with

Table 2. Metabolites changed in acute radiation enteritis (ARE) model (negative ion mode).

| Name | Description | VIP | Fold change | P-value |
|------------|---|---------|-------------|----------|
| M242T458 | Cytidine | 1.01366 | 2.273262 | 0.000211 |
| M103T385 | 2-hydroxy-butanoic acid | 1.04305 | 1.766476 | 0.017277 |
| M111T163 | Uracil | 1.98626 | 1.763974 | 0.029072 |
| M199T88 | Dodecanoic acid | 2.89737 | 1.715666 | 0.00509 |
| M103T466 | D(-)-beta-hydroxy butyric acid | 1.55693 | 1.630876 | 0.022899 |
| M154T748 | L-Histidine | 2.93701 | 1.4856 | 0.020178 |
| M303T78 | Arachidonic Acid (peroxide free) | 8.83898 | 1.428324 | 0.01473 |
| M331T77 | Adrenic Acid | 3.22814 | 1.420699 | 0.017129 |
| M116T571 | L-Valine | 1.36692 | 1.403015 | 0.001152 |
| M226T393 | Deoxycytidine | 1.60153 | 1.332033 | 0.002327 |
| M89T495 | DL-lactate | 1.01463 | 1.318664 | 0.03806 |
| M164T482 | L-Phenylalanine | 1.56677 | 1.29007 | 0.008941 |
| M130T496 | L-Isoleucine | 1.96772 | 1.284513 | 0.032208 |
| M141T651_1 | 2-Oxo adipic acid | 3.979 | 0.909297 | 6.54E-05 |
| M307T79 | 11(Z),14(Z)-Eicosadienoic Acid | 1.20875 | 0.800079 | 0.042495 |
| M213T291 | m-Chlorohippuric acid | 1.00371 | 0.775288 | 0.018977 |
| M161T588 | D-Tagatose | 1.28494 | 0.743228 | 0.000713 |
| M114T593 | L-Proline | 1.0367 | 0.734349 | 0.00015 |
| M179T573 | Alpha-D-Glucose | 5.19967 | 0.704439 | 0.001102 |
| M212T54 | Indoxyl sulfate | 6.63785 | 0.610939 | 0.006602 |
| M297T89 | Nname,cis-9,10-Epoxy stearic acid | 1.44621 | 0.610299 | 0.042923 |
| M71T588 | Dihydroxyacetone | 3.82948 | 0.593026 | 0.000439 |
| M432T182 | Glycolithocholic acid | 3.03497 | 0.544063 | 0.003026 |
| M295T88_2 | 13(S)-HODE | 2.281 | 0.515801 | 0.002587 |
| M182T78 | 4-Pyridoxic acid | 1.05022 | 0.509796 | 0.001129 |
| M465T51 | Cholesterol 3-sulfate | 2.51353 | 0.411366 | 0.019309 |
| M177T199 | L-Gulonic gamma-lactone | 8.43768 | 0.399621 | 0.000332 |
| M451T292 | Chenodeoxycholate | 2.05113 | 0.348401 | 0.001598 |
| M174T744 | L-Citrulline | 1.33624 | 0.262892 | 7.93E-09 |
| M188T203 | 3-Indolepropionic acid | 7.74442 | 0.250502 | 4.43E-07 |
| M407T431 | Cholic acid | 2.16337 | 0.227481 | 2.73E-05 |
| M186T211 | Indoleacrylic acid | 2.72592 | 0.216533 | 3.01E-09 |
| M153T51 | 3,4-Dihydroxybenzoate (Protocatechuic acid) | 2.01679 | 0.202945 | 1.76E-13 |
| M137T72 | Salicylic acid | 1.39911 | 0.186419 | 1.08E-10 |
| M178T379 | Hippuric acid | 1.81315 | 0.102516 | 5.89E-11 |

VIP, the variable importance in the projection.

metabolites profiles of intestinal tissues is performed, the results may be more meaningful. In addition, all data in this study are obtained based on animal samples, which need validation in human samples.

In summary, we observed profiles of serum metabolites in ARE. Several differentially expressed serum metabolite were found as potential diagnostic biomarkers of ARE, and the pathways responsible for ARE development were also explored. These results may provide latent clues for ARE related research and less invasive diagnosis.

Acknowledgments

This work was supported by Natural Science Foundation of China (No. 81773227), Top Talent Support Program for young and middle-aged people of Wuxi Health Committee (HB2020009), High-end talents of 2020 Taihu Talent Program High-end medical expert team of the 2020 Taihu Talent Plan.

Conflict of Interest

The authors declare no conflict of interest.

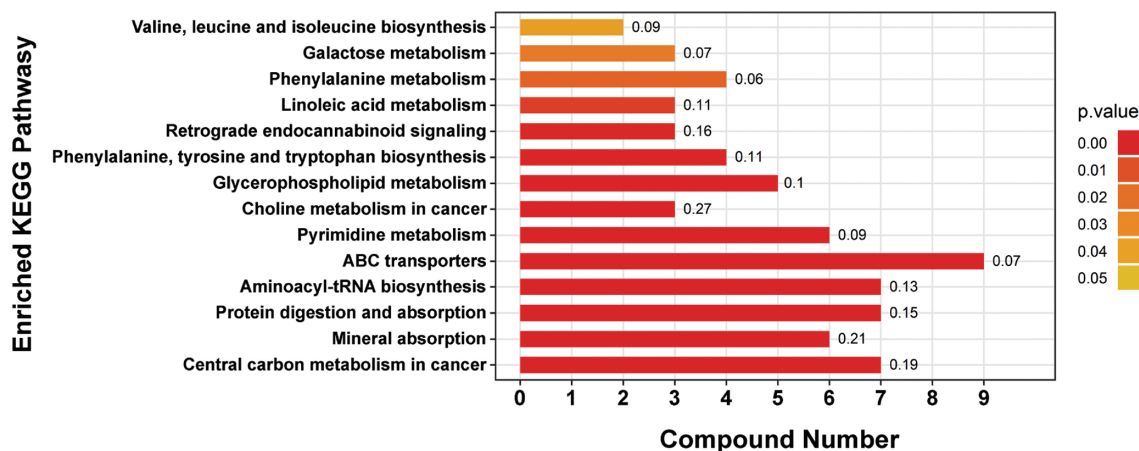


Fig. 5. Pathways related to identified metabolites.

Kyoto Encyclopedia of Genes and Genome (KEGG) analysis enriched all identified metabolites into 14 different pathways. Numbers after each column represent the rich factors.

References

- Abshire, D. & Lang, M.K. (2018) The evolution of radiation therapy in treating cancer. *Semin. Oncol. Nurs.*, **34**, 151-157.
- Alakwaa, F.M., Chaudhary, K. & Garmire, L.X. (2018) Deep learning accurately predicts estrogen receptor status in breast cancer metabolomics data. *J. Proteome Res.*, **17**, 337-347.
- Ashburn, J.H. & Kalady, M.F. (2016) Radiation-induced problems in colorectal surgery. *Clin. Colon Rectal Surg.*, **29**, 85-91.
- Atya, H.B., Ali, S.A., Hegazy, M.I. & El Sharkawi, F.Z. (2018) Urinary urea, uric acid and hippuric acid as potential biomarkers in multiple sclerosis patients. *Indian J. Clin. Biochem.*, **33**, 163-170.
- Broin, P.O., Vaitheesvaran, B., Saha, S., Hartil, K., Chen, E.I., Goldman, D., Fleming, W.H., Kurland, I.J., Guha, C. & Golden, A. (2015) Intestinal microbiota-derived metabolomic blood plasma markers for prior radiation injury. *Int. J. Radiat. Oncol. Biol. Phys.*, **91**, 360-367.
- Brown, D.G., Rao, S., Weir, T.L., O'Malia, J., Bazan, M., Brown, R.J. & Ryan, E.P. (2016) Metabolomics and metabolic pathway networks from human colorectal cancers, adjacent mucosa, and stool. *Cancer Metab.*, **4**, 11.
- Chen, S., Kong, H., Lu, X., Li, Y., Yin, P., Zeng, Z. & Xu, G. (2013) Pseudotargeted metabolomics method and its application in serum biomarker discovery for hepatocellular carcinoma based on ultra high-performance liquid chromatography/triple quadrupole mass spectrometry. *Anal. Chem.*, **85**, 8326-8333.
- Fan, Y. & Pedersen, O. (2021) Gut microbiota in human metabolic health and disease. *Nature reviews. Microbiology*, **19**, 55-71.
- Hauer-Jensen, M., Wang, J., Boerma, M., Fu, Q. & Denham, J.W. (2007) Radiation damage to the gastrointestinal tract: mechanisms, diagnosis, and management. *Curr. Opin. Support. Palliat. Care*, **1**, 23-29.
- Isomura, M., Oya, N., Tachiiri, S., Kaneyasu, Y., Nishimura, Y., Akimoto, T., Hareyama, M., Sugita, T., Mitsuhashi, N., Yamashita, T., Aoki, M., Sai, H., Hirokawa, Y., Sakata, K., Karasawa, K., et al. (2008) IL12RB2 and ABCA1 genes are associated with susceptibility to radiation dermatitis. *Clin. Cancer Res.*, **14**, 6683-6689.
- Johnson, C., Ivanisevic, J. & Siuzdak, G. (2016) Metabolomics: beyond biomarkers and towards mechanisms. *Nature reviews. Molecular cell biology*, **17**, 451-459.
- Jones, J.W., Jackson, I.L., Vujaskovic, Z., Kaytor, M.D. & Kane, M.A. (2017) Targeted metabolomics identifies pharmacodynamic biomarkers for BIO 300 mitigation of radiation-induced lung injury. *Pharm. Res.*, **34**, 2698-2709.
- Khalid, U., McGough, C., Hackett, C., Blake, P., Harrington, K.J., Khoo, V.S., Tait, D., Norman, A.R. & Andreyev, H.J. (2006) A modified inflammatory bowel disease questionnaire and the Vaizey Incontinence questionnaire are more sensitive measures of acute gastrointestinal toxicity during pelvic radiotherapy than RTOG grading. *Int. J. Radiat. Oncol. Biol. Phys.*, **64**, 1432-1441.
- Kurland, I.J., Broin, P.O., Golden, A., Su, G., Meng, F., Liu, L., Mohney, R., Kulkarni, S. & Guha, C. (2015) Integrative metabolic signatures for hepatic radiation injury. *PLoS One*, **10**, e0124795.
- Laiakis, E.C., Hydeke, D.R. & Fornace, A.J. (2012) Comparison of mouse urinary metabolic profiles after exposure to the inflammatory stressors gamma radiation and lipopolysaccharide. *Radiat. Res.*, **177**, 187-199.
- Li, J., Yang, L., Li, Y., Tian, Y., Li, S., Jiang, S., Wang, Y. & Li, X. (2015) Metabolomics study on model rats of chronic obstructive pulmonary disease treated with BuFei JianPi. *Mol. Med. Rep.*, **11**, 1324-1333.
- Li, L., Wang, C., Yang, H., Liu, S., Lu, Y., Fu, P. & Liu, J. (2017a) Metabolomics reveal mitochondrial and fatty acid metabolism disorders that contribute to the development of DKD in T2DM patients. *Mol. Biosyst.*, **13**, 2392-2400.
- Li, P., Wuthrick, E., Rappaport, J.A., Kraft, C., Lin, J.E., Marszalowicz, G., Snook, A.E., Zhan, T., Hyslop, T.M. & Waldman, S.A. (2017b) GUCY2C signaling opposes the acute radiation-induced GI syndrome. *Cancer Res.*, **77**, 5095-5106.
- Liu, L.L., Lin, Y., Zhuang, J.C., Ren, J., Jiang, X.Y., Chen, M.H., Chen, W., Luo, X., Yan, J.H., Niu, J.J. & Yang, T.C. (2019) Analysis of serum metabolite profiles in syphilis patients by untargeted metabolomics. *J. Eur. Acad. Dermatol. Venereol.*, **33**, 1378-1385.
- Ni, Y., Su, M., Lin, J., Wang, X., Qiu, Y., Zhao, A., Chen, T. & Jia, W. (2008) Metabolic profiling reveals disorder of amino acid metabolism in four brain regions from a rat model of chronic unpredictable mild stress. *FEBS Lett.*, **582**, 2627-2636.
- Nicholls, A., Mortishire-Smith, R. & Nicholson, J. (2003) NMR spectroscopic-based metabolomic studies of urinary metabolite variation in acclimatizing germ-free rats. *Chem. Res. Toxicol.*, **16**, 1395-1404.
- Oxenkrug, G., van der Hart, M., Roeser, J. & Summergrad, P. (2016) Anthranilic acid: a potential biomarker and treatment target for schizophrenia. *Ann. Psychiatry Ment. Health*, **4**, 1059.
- Oxenkrug, G., van der Hart, M. & Summergrad, P. (2015) Elevated anthranilic acid plasma concentrations in type 1 but not type 2 diabetes mellitus. *Integr. Mol. Med.*, **2**, 365-368.

- Pannkuk, E.L., Fornace, A.J. Jr. & Laiakis, E.C. (2017) Metabolomic applications in radiation biodosimetry: exploring radiation effects through small molecules. *Int. J. Radiat. Biol.*, **93**, 1151-1176.
- Shi, H., Li, X., Zhang, Q., Yang, H. & Zhang, X. (2016) Discovery of urine biomarkers for bladder cancer via global metabolomics. *Biomarkers*, **21**, 578-588.
- Stacey, R. & Green, J.T. (2014) Radiation-induced small bowel disease: latest developments and clinical guidance. *Ther. Adv. Chronic Dis.*, **5**, 15-29.
- Sun, Y., Saito, K., Iiji, R. & Saito, Y. (2019) Application of ion chromatography coupled with mass spectrometry for human serum and urine metabolomics. *SLAS Discov.*, **24**, 778-786.
- Sun, Y., Xing, X., Liu, Q., Wang, Z., Xin, Y., Zhang, P., Hu, C. & Liu, Y. (2015) Hypoxia-induced autophagy reduces radiosensitivity by the HIF-1alpha/miR-210/Bcl-2 pathway in colon cancer cells. *Int. J. Oncol.*, **46**, 750-756.
- Wilson, T., Garcia-Perez, I., Posma, J.M., Lloyd, A.J., Chambers, E.S., Tailliant, K., Zubair, H., Beckmann, M., Mathers, J.C., Holmes, E., Frost, G. & Draper, J. (2019) Spot and cumulative urine samples are suitable replacements for 24-hour urine collections for objective measures of dietary exposure in adults using metabolite biomarkers. *J. Nutr.*, **149**, 1692-1700.
- Zhang, Y., Zhou, X., Li, C., Wu, J., Kuo, J.E. & Wang, C. (2014) Assessment of early triage for acute radiation injury in rat model based on urinary amino acid target analysis. *Mol. Biosyst.*, **10**, 1441-1449.
- Zhao, M., Lau, K.K., Zhou, X., Wu, J., Yang, J. & Wang, C. (2017) Urinary metabolic signatures and early triage of acute radiation exposure in rat model. *Mol. Biosyst.*, **13**, 756-766.
-